Journal of Thermal Analysis and Calorimetry, Vol. 78 (2004) 7–31

THE TRIBULATIONS AND SUCCESSES ON THE ROAD FROM DSC TO TMDSC IN THE 20TH CENTURY THE PROSPECTS FOR THE 21ST CENTURY*

Bernhard Wunderlich[**]

Department of Chemistry, The University of Tennessee, Knoxville, TN 37886-1600, and Chemical Sciences Division, Oak Ridge National Laboratory, Oak Ridge, TN, USA

Abstract

All started with the invention of differential thermal analysis, DTA at the beginning of the 20th century. The tool was qualitative in the measurement of heat, but quantitative in measuring temperature. The differential scanning calorimetry, DSC, became popular in the 1970s. In certain temperature regions, it could replace even the more precise, but cumbersome, classical technique of adiabatic calorimetry. A large volume of quantitative thermodynamic information was accumulated. Both equilibrium and non-equilibrium data were collected. Unfortunately, the qualitative applications of the DSC grew even faster and overshadowed the quantitative capabilities of measurement of heat. The newer temperature-modulated DSC, TMDSC, makes use of the same instrumentation and seems to follow the same fate, despite the fact, that it can distinguish equilibrium from non-equilibrium, a key information needed in the thermodynamic description of materials. Seeing the growth of these efficient techniques, one could conclude that all questions one might have wanted to ask in 1900 can be answered now. A new question, however, has become important in the 21st century: What happens at the nanophase level and in the description of very fast processes? Are we able to learn from the past, or are we again to stay at the level of qualitative DTA?

Keywords: baseline, DSC, DTA, glass transition, heat capacity, melting transition, microcalorimetry, nanophase, phase, reversible melting, reversing melting, temperature-modulated DSC, thermodynamics, TMDSC

Introduction (Phases, Molecules, and Thermal Analysis)

To understand the basis of quantitative thermal analysis, it is necessary to develop a set of descriptions for phases and molecules that allows an identification of the materials to be analyzed [1]. Figure 1 illustrates a schematic of the condensed phases as developed on the discovery of the conformationally disordered crystals (condis crystals), about 20 years ago [2]. The five solid phases increase in order from the amorphous glass to the crystal. All of these solids have practically only inter- and intra-molecular, vibrational, small-amplitude motion. All incompletely ordered sol-

* Summary of a lecture to the Ohio Valley Thermal Analysis Society on August 18, 2003.

** Author for correspondence: E-mail: athas@utk.edu

1388–6150/2004/ $ 20.00

Akadémiai Kiadó, Budapest
Kluwer Academic Publishers, Dordrecht

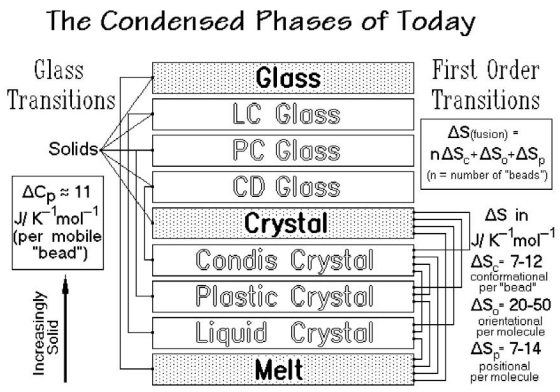

Fig. 1 Schematic of the various types of condensed phases, their nature, connecting transitions, and thermodynamic characterization [2]

ids change on heating to the corresponding mobile phase at their respective characteristic glass transitions (a transition without a heat and entropy of transition), indicated by the connecting lines on the left. In the melt, one can find all types of large-amplitude molecular motion in addition to the molecular vibrations permitted by the molecular structure of the molecules. The large-amplitude motions are characterized as translation (positional motion), rotation (orientational motion), and internal rotation (conformational motion). The liquid, plastic, and condis crystals are mesophases of decreasing mobility and increasing order. Liquid crystals possess some orientational order, but no positional and conformational order. Plastic crystals possess full positional order, but no orientational order and usually incomplete conformational order. Condis crystals have positional and orientational order, but incomplete conformational order. On cooling, the increasing amount of order on going from the melt to the crystal leads to the various first order transitions (transitions with a heat and entropy of transition), as indicated by the connecting lines on the right. In certain cases the mesophase order may also change gradually without a transition. Thermal analysis allows a classification of the phases by establishing the entropies of the first order transitions, as marked on the right (ratio of the latent heat to the equilibrium transition temperature), or by finding the changes in heat capacity during the glass transitions and comparing it to empirical values of similar compounds, as marked on the left. Macroscopic, quantitative thermal analysis, thus, is linked to the microscopic molecular structure and motion.

All possible molecules are classified in Fig. 2 and connected to their possible phase structures [3]. The large molecules (macromolecules) consist of more than 1 000 atoms, as suggested by Staudinger (Nobel Prize in 1953 for the development of the theory of macromolecules in the 1920s). This definition was chosen since relatively few molecules with about 1 000 atoms are known. Furthermore, once the macromolecular size has been reached, most properties change only little with additional increases in size. Macromolecules cannot be brought into the gas phase. The

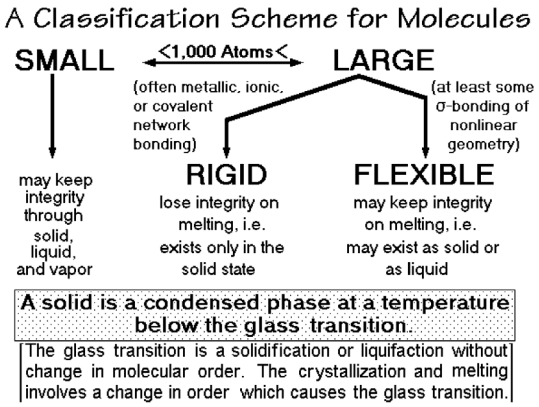

Fig. 2 Classification of molecules and an operational definition of the solid-state [3]

kinetic energy needed in the condensed state to separate such large molecules from their neighbors for evaporation is so high, that decomposition occurs. The subdivision into rigid and flexible macromolecules is useful since only the flexible macromolecules (often called simply polymers) may attain a high-entropy liquid state without losing molecular integrity.

The definition of the solid-state at the bottom of Fig. 2 is a logical result based on the discussion of Fig. 1. A melt can turn into a solid by lowering the temperature through the glass transition temperature which freezes the large-amplitude motion. Similarly, crystallization of the melt freezes the cooperative, large-amplitude motion by an increase in order of the packing of the molecules. In both cases a solid results with predominantly vibrational, small-amplitude motion. The glass transition occurs usually at a lower temperature than crystallization.

A final point needs to be made. In the same fashion that molecules may range from large to small, phases may change from large, bulk phases, also called macrophases, to microphases, and finally to nanophases [4]. Thermodynamically, the macrophases are described by the heat capacity, $C_p=(\partial H/\partial T)_{p,n}$ and the latent heats of transition $L=(\partial H/\partial n)_{p,T}$. From the heat capacities and latent heats the integral functions, enthalpy, H, entropy, S, and free enthalpy, G can be derived. A direct connection to the molecular motion is indicated in Fig. 1 and discussed further with Fig. 8, below. The enthalpy H is the total heat content of the sample, and S and G are a measure of the degree of order and the thermodynamic stability, respectively. Microphases are less than about one micrometer in size. For their thermodynamic description, the specific surface free energy, σ in J cm^{-2}, needs to be considered because of the large specific surface area of the smaller phase. For example, the melting temperature lowering, ΔT, of lamellar crystals of microphases, as found for folded-chain crystals of polymers, is described by the Gibbs–Thomson equation [$\Delta T = 2\sigma T_m^o/(\Delta H_f' l)$, where T_m^o is the equilibrium melting temperature of the macrophase, $\Delta H_f'$ is the heat of fusion in J cm^{-3}, and l, the lamellar thickness in cm [5]. Flexible macromolecules may be longer than one micrometer and it is possible that they can

cross phase boundaries and cause strong bonds between different microphases, a characteristic of many polymer samples. The final phase type, the nanophase is much smaller than a flexible macromolecule. For a definition of their size, one can propose that the surface effects cross the whole nanophase, excluding the existence of any bulk material within the nanophase [6]. Typical examples of such nanophases are semicrystalline polymers in which a part of the noncrystalline material exists as a rigid-amorphous fraction with a glass transition higher than that of the bulk-amorphous phase [7]. The much longer macromolecules may participate in a number of different phases.

Combining all the definitions of importance for the description of the condensed phase, one can expect nine phases with three different sizes, and three types of molecules. This variety of 81 situations is to be identified by thermal analysis. A detailed inspection reveals that not all combinations may be possible, but at least 57 different combinations can be expected, a sufficient number to require careful specification, possible by quantitative thermal analysis [4].

Instrumentation (DTA, DSC, TMDSC)

The tribulations and successes of thermal analysis in the 20th century are based on the work done in the 18th and 19th century using thermometry [1]. Figure 3 illustrates a schematic of the earliest thermal analysis equipment. It can be used to produce heating or cooling curves. The heating curve shown has the goal to establish a phase diagram. Note that in this experiment the determination of temperature is already quantitative since the temperature is measured inside the sample. Its precision even may be higher than in present-day thermal analysis which relies on measurements outside of the sample container. The evaluation of the heat flow from heating and cooling curves is more difficult. The heat flow over a small range of change in temperature can be judged from Newton's law, as written in Fig. 3, where T_o is the

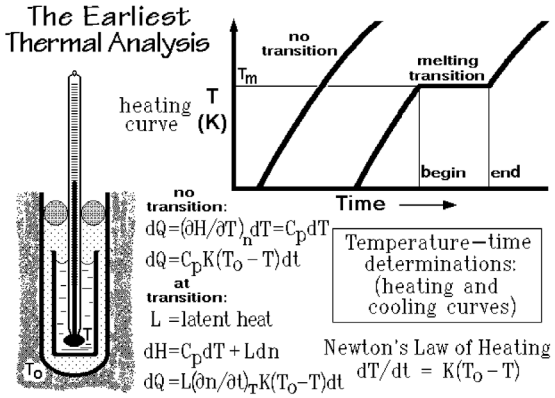

Fig. 3 Early thermal analysis in form of heating curves for the quantitative determination of phase diagrams, based on Newton's law [1]

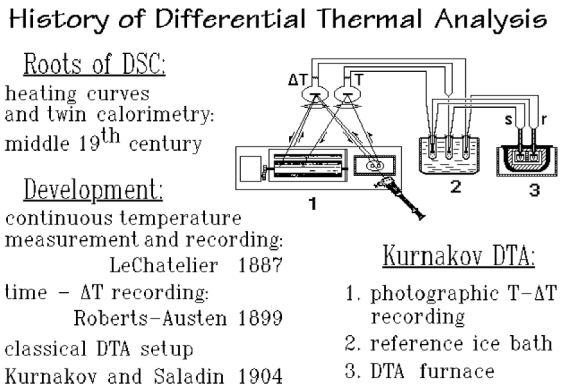

Fig. 4 Early 20th century DTA as developed by Kurnakov in 1904 [1]

temperature of the environment and K is a constant. The heating rate, dT/dt is a linear function of the temperature difference. During melting, the temperature is constant, as for example at the eutectic temperature, T_e. The heat flow is now due to the latent heat and dQ can be determined, as shown in the figure. Both, information on the heat capacity and on latent heat can be extracted by calibration of K.

Figure 4 illustrates the first step toward the solution of the difficult calibration problem. It became possible at the beginning of the 20th century by the development of differential thermal analysis, DTA [8]. Two different measurements are made simultaneously, approximately separating the effect of the sample from the environment by determining ΔT, the difference in temperature between reference, r, and sample, s, as a function of temperature, T, and time, t. A typical DTA trace, taken many years later, is shown in Fig. 5. In the fingerprinting technique, the transition temperatures are determined for characterization. Again these temperatures were quantitative because the thermocouple could be placed in the sample. Now, calibrat-

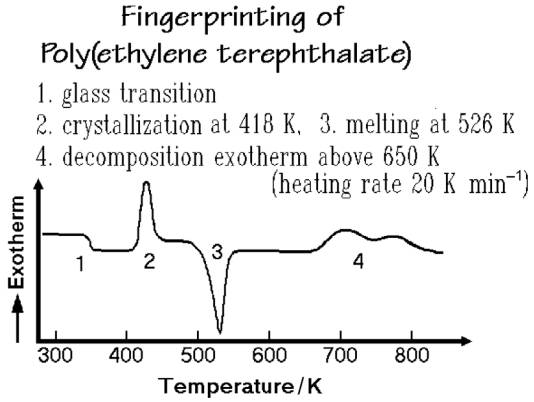

Fig. 5 Qualitative DTA used for 'fingerprinting' to characterize materials, in this case poly(ethylene terephthalate) [1]

ing the area of a ΔT *vs*. T, or better ΔT *vs*. t plot to obtain quantitative heat-flow rates is easier, but still separate runs under identical conditions were needed for calibration. A three-run technique was developed which is still necessary today for quantitative measurements [9]. This calibration was, however, not always precise until the sample mass could be reduced to about 10 mg or less, so that container and sample would not differ much in temperature and the thermometer could be placed outside of the sample container and, thus, the heat measurements are more reproducible from run to run. This new type of DTA was called a differential scanning calorimeter, DSC [10].

A further advance in the DSC began with the commercial development of a temperature-modulated DSC, TMDSC [11]. Figure 6 illustrates a modern DSC, capable of temperature modulation. Two modes of calculations for the specific heat capacity are given by the boxed equations. The measurement in the DSC mode is identical to the old DTA analysis. Figure 7 illustrates on the left the change in sample, reference, and block temperatures, T_s, T_r, and T_b, respectively. As soon as steady state is achieved, after about 100 s, the DSC result can be computed based on the linearity of Newton's law of Fig. 2. The difference in temperature, $\Delta T = T_r - T_s$, is proportional to the heat-flow rate. The calibration is done by the three-run method, as before. The remaining uncertainties involve the temperature gradient within the sample and the differences in the slopes of the three temperatures with time because of changes in heat capacities. The first uncertainty is small for the measurement of heat capacity, but becomes excessive during the absorption or evolution of large latent heats during transitions.

Special methods are available to establish the latent heat via the 'baseline-method' [1], the kinetics of the transitions, however, cannot be determined with a fixed heating rate because of excessive instrument lags during sharp transition peaks [12]. The second part of the DTA or DSC equation in Fig.6 corrects for the changes in c_p and does not need additional measurement. Unfortunately, this small correction is usually omitted in commercial software.

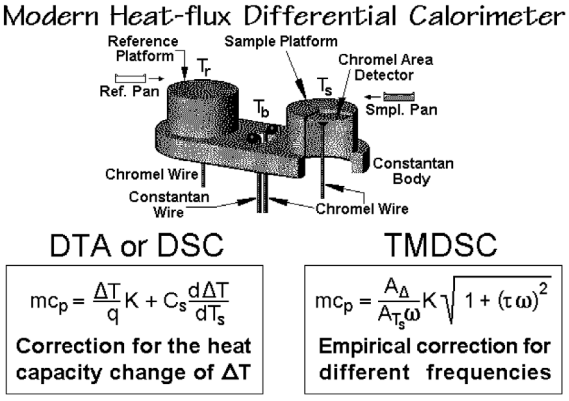

Fig. 6 Modern DSC as developed by T. A. Instruments Inc. in 2001, capable of performing temperature-modulated DSC [11]

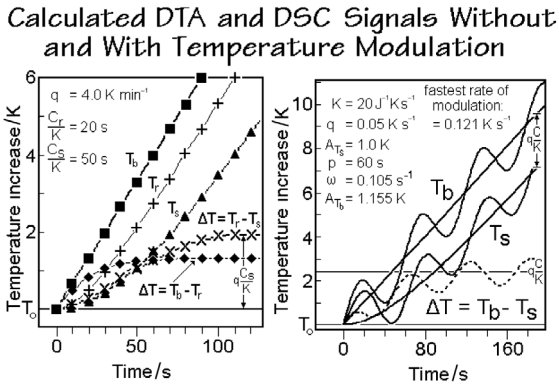

Fig. 7 Computed temperatures in a DSC and TMDSC and the corresponding response

The second mode of measurement is that of the TMDSC. A sinusoidal change temperature is superimposed on the underlying standard DSC, as indicated in the right curves of Fig. 7. Naturally, forming a sliding average over one sinusoidal modulation period, p, yields the shown underlying changes in temperature. These cause the underlying heat-flow-rate responses through ΔT and can be used, as in the standard DSC, for calculation of the total heat capacity. As long as the calorimeter, including the sample, remains at steady state and has a linear response during all the changes in heating rates, an analogous averaging as done with the sample temperature can be used to deconvolute the underlying heat-flow rate and the reversing heat-flow rate [13]. This process allows to calculate the reversing heat capacity in addition to the total heat capacity, as shown in Fig. 6. The temperature difference ΔT is replaced by the amplitude of the temperature difference A_Δ, and the heating rate $q \approx \mathrm{d}T_s/\mathrm{d}t$ is replaced by $A_{Ts}\omega$, the amplitude of the heating rate with ω representing the frequency in units of $2\pi/p$. Both amplitudes are usually found by fitting a Fourier series to the signals. The calibration constant K is again determined by the three-run method, and the square-root expression indicates the change with frequency. In the usual case that steady state is lost, it is best to treat τ as a second parameter and establish its value by measuring at different frequencies [14]. At high frequencies, τ becomes dependent on frequency ω itself. With well established values of τ a precision of $\pm 0.1\%$ in heat capacity could be reached [15].

Reversible heat capacity and latent heat contributions give the same results in standard DSC and TMDSC. If there is an irreversible response, the two are different and need to be studied, as will be discussed below. A note to nomenclature: It is useful to apply the term 'reversing' to the raw data from the modulated response. These may still need to be corrected for effects caused by irreversible processes or for errors in the method of deconvolution. The term 'reversible' is to be used only after the data analysis has shown that true, thermodynamic reversibility exists.

Standard and Temperature-modulated Calorimetry (Run Parameters and Analyses)

For the standard DSC the run parameters were mentioned in the previous section. An extensive number of applications have been described [16], and a special summary of selected quantitative analyses has been presented [17]. In Fig. 8, an example of the analysis of the heat capacity of polyethylene is given, based on adiabatic calorimetry and standard DSC methods [18,19]. The top curve represents the normal mode spectrum of the vibrations of crystalline polyethylene. The left portion accounts for the skeletal vibrations that include all intermolecular vibrations and the bending and torsional vibrations of the C–C-backbone. Their contribution to the heat capacity is shown in the bottom curve after fitting to the low-temperature heat capacity with an appropriate Tarasov function (for information see the ATHAS Data Bank [20]). At room temperature, these skeletal vibrations are fully excited. The larger number of group vibrations contributes little to the heat capacity at low temperature, but account for most of the increases in C_p at higher temperature. Adding both contributions and changing from the heat capacity at constant volume (C_v to C_p), the total heat capacity is calculated. It agrees with the experimental data up to about 250 K. Above this temperature large-amplitude motion involved in the equilibrium of the gauche defects becomes active, as can be deduced from the small increase in heat capacity beyond the calculated total C_p. By computer simulation, it could be determined that the gauche defects had a lifetime of about one picosecond (10^{-12} s) and their concentration reaches about 2% at the melting temperature (414.6 K) [21, 22]. The ATHAS Data Bank contains such information on more than 100 polymer and links molecular motion to heat capacity [20]. Of special value is the observation of the beginning of large-amplitude motion. It is connected with the mechanical properties of the polymers. For glassy polyethylene a similar increase in heat capacity as seen in Fig. 8 is observed starting at about 120 K, below the major portion of the glass transition at 237 K. It has also been linked to localized gauche-trans equilibria. Such analyses of

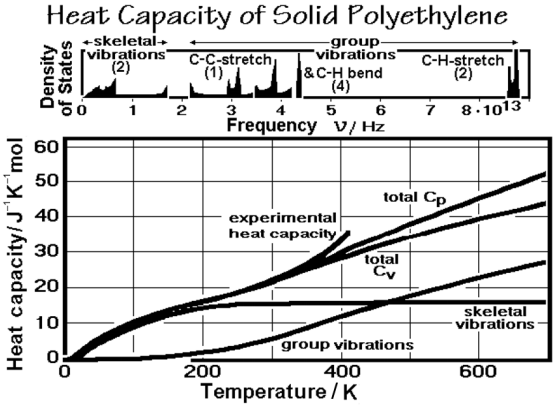

Fig. 8 Densities of vibrational states in solid polyethylene and the connection to heat capacity [19]

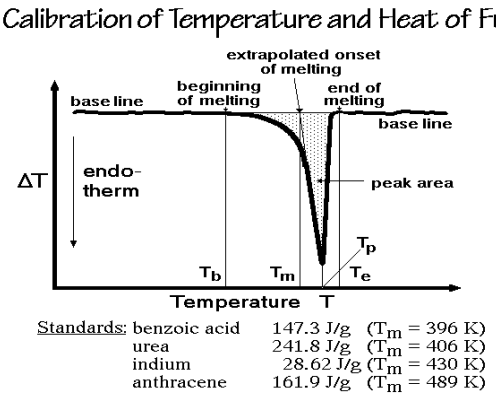

Fig. 9 Quantitative data on melting temperature and heat of fusion (latent heat) [1]

the heat capacity give a quantitative baseline for an analysis of the changes of the properties of the polymers with temperature and ultimately permit quantitative separation of latent heat effects from C_p.

Figure 9 illustrates a simple calibration trace using a sharply melting standard with a temperature difference between the end of melting and the beginning of melting of, perhaps, 1–3 K. In the indicated case, a linear connection between the beginning and end of melting is sufficient to quantitatively evaluate the peak area in terms of the latent heat by the baseline method, which consists of an integration of the heat-flow rate over time [9]. The slope of the line from the peak to the onset of melting in such a plot of ΔT *vs*. time should be equal to the heating rate q if no undue lags exist. In the shown plot of ΔT *vs*. temperature of the sample, the slope is due to the lag of the calorimeter and is often used for an approximate lag correction, although the lag will change somewhat with the nature of the sample. The extrapolated onset of melting is a good approximation of the equilibrium melting temperature. In this way, both, temperature and latent heat can be calibrated or measured quantitatively.

In case the melting occurs over a much broader temperature range, let us say 20 to 100 K, as is common for semicrystalline polymers, the baseline must be considered in terms of its detailed heat capacity components arising from the solid and melt. Figure 10 contains a schematic drawing of a baseline in terms of the heat capacity. The apparent heat capacity $C_p^\#$ is the sum of the thermodynamic heat capacity and the effect of the latent heat. The fractions indicate the amounts melted in terms of the latent heat absorbed, which can be expressed as the changing crystallinity, w_c. In addition to the change of the heat capacity with temperature, the heat of fusion itself changes with temperature, as indicated by Eq. (1) in Fig. 10. Equation (2) is then the description of the apparent heat capacity, $C_p^\#$. Finally, Eq. (3) eliminates C_{pc} as a variable for an easy calculation of w_c, using only the measured curve for $C_p^\#$, the extrapolation of C_{pa} from measurement above the melting point to the temperature of interest, and the data for the change of the latent heat with temperature, as given in the ATHAS Data Bank [20].

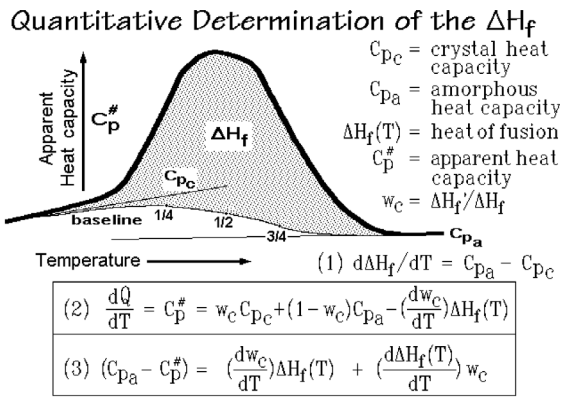

Fig. 10 Quantitative determination of the crystallinity as a function of temperature

The large volume of quantitative information gained by DSC is now to be extended by the use of TMDSC. A number of additional parameters need to be considered for quantitative determination of the reversing and reversible heat-flow rates [23]. Figure 11 shows a summary of five basic segments out of which a periodic change in temperature can be generated. For the simple modulation of Fig. 7, identical sinusoidal segments were combined with a positive ramp of increasing temperature. The center curve in Fig. 11 illustrates a simple addition of positive and negative ramps for sawtooth modulation. Such modulation can be described by a sum of sinusoidal, odd-numbered Fourier harmonics with decreasing amplitudes. Each of the harmonics can be treated as indicated in Fig. 6, i.e., one can conduct simultaneously a number of experiments with different frequencies, ω [24] as illustrated in Figs 19 and 20, below. Similarly, the step-wise heating and cooling as represented at the bottom of Fig. 11 and any other periodic function can be separated into a series of sinusoidal harmonics and used in frequency dependent TMDSC. Figure 12 illustrates a complex

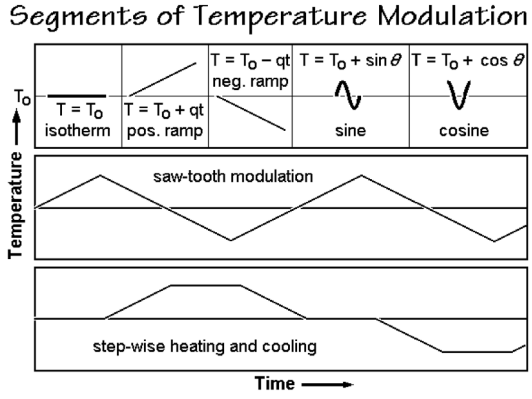

Fig. 11 Types of modulation for TMDSC

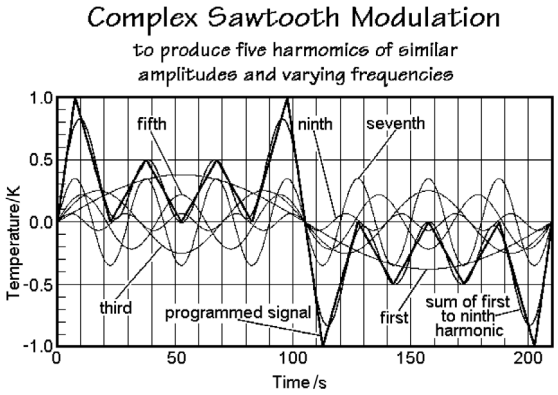

Fig. 12 Complex sawtooth modulation and the harmonics for the Fourier series describing the modulation [14]

sawtooth and its harmonics that are useful because of its ease of programming out of 14 linear segments. Its advantages lie in the similar amplitudes of the different harmonics and the limited number of harmonics which represent almost the complete programmed signal. For a sufficiently long first harmonic period, it is even possible to use the linear segments for evaluation with the standard DSC technique.

The analysis of a sinusoidal harmonic is illustrated in Fig. 13 for the heat-flow-rate amplitude, A_Δ. An identical treatment can be used for the modulated temperature, A_{Ts}. Curve C is the reversing heat-flow-rate response after subtracting the underlying effect (B) from the recorded curve (A). Curves A and B are not shown. A detailed discussion and a spread-sheet program for such analysis are available [13, 25]. Curves D and E are the two components of C which define the phase difference from the sample temperature, F and G identify the amplitudes of the respective com-

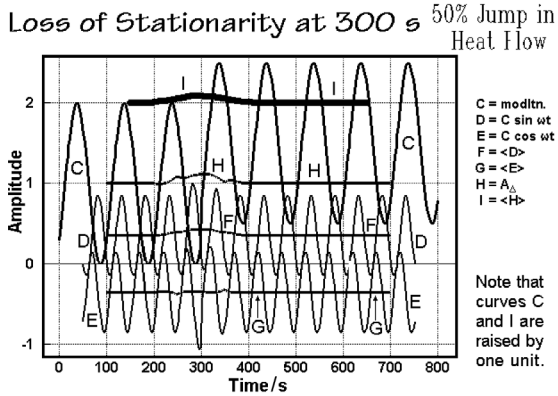

Fig. 13 Analysis of a single, sinusoidal modulation with a jump in irreversible contribution at 300 s into the experiment

ponents and can be used to establish the amplitude A_Δ which is often further smoothed to yield the TMDSC output for A_Δ, curve I. Some 300 s into the experiment an irreversible heat-flow rate of the enormous amount of 50% is added, simulating a shift in the baseline as may be caused by a major change in the purge gas pressure, a constant chemical reaction, shift in the sample, deformation of the sample pan, etc. Curves H and I illustrate that there is only a small, temporary disturbance in the reversing heat-flow-rate amplitude. After a short time, the reversing signal has reached its old value, indicating that the shift is not reversible. For the time period immediately preceding and following the disturbance, the deconvolution by averaging over one modulation period is not stationary, i.e., the reversing heat-flow rate, not being sinusoidal, does not give a zero contribution to the total heat-flow rate, as was assumed above. This nonstationary response will cause problems in the analysis of melting by TMDSC. Curve C as plot of time, however, allows a full analysis of the change of the calorimeter response. Figure 14 illustrates a more gradual irreversible change as one may find during irreversible sublimation or a slowly increasing chemical reaction. The upper curves come from a linear increase, beginning at 250 s, the lower ones from an exponential increase, beginning at time zero. The reversing response is showing practically nothing of the growing irreversible effect, suggesting that reversible effects such as heat capacities can still be measured with reasonable precision in the presence of large, irreversible processes as long as stationarity is preserved.

After enumerating the various tribulations caused by the need for proper calibration and observation of linear response, steady state, temperature gradients, thermal resistance, stationarity, and instrument lag that need to be overcome to do quantitative DTA, DSC, and TMDSC, a brief accounting will be given next for the new successes of TMDSC of solid polymers. A full accounting of this topic is available [26]. From this discussion, one can conclude that quantitative TMDSC created more tribulations than DSC, but yields also additional great successes.

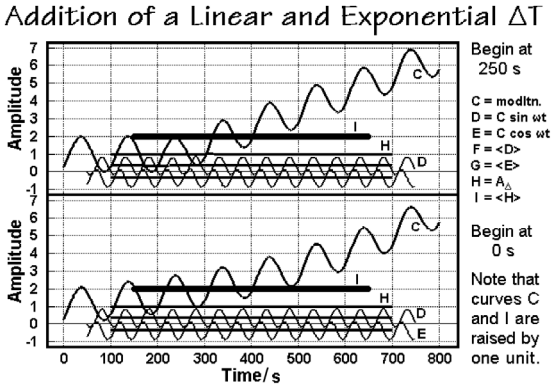

Fig. 14 Separation of a linear and an exponential irreversible contribution from the reversing signal (upper and lower curves, respectively)

Melting, Heat Capacity, and Glass Transitions

A textbook example of a TMDSC trace is poly(ethylene terephthalate), PET. Figure 15 shows the raw data of an initially amorphous sample of PET similar to the simple fingerprint in Fig. 5. The top curve displays the change in heat-flow rates during the glass transition, cold crystallization, reorganization, and melting. The bottom curve shows the modulated heating rate, chosen such that the sample is never cooled, i.e., crystallization can never be induced by cooling. Thus, such modulations with underlying, linear heating rates that match the modulation during the cooling cycle avoid any possible reversible crystallization of the sample after melting. Any exotherm observed, as in Fig. 15 between 470 and 530 K, must then arise from irreversible processes.

The first observation in Fig. 15 is that in the melting region from 500 to about 530 K the heating rate does not follow the program which means, the interpretation of the data in this temperature range is questionable. Second, the cold crystallization is almost completely separated from the reversing signal. It is fully irreversible since the crystallization rate is nearly constant during the changing temperature and for the analysis, the beginning and end of the crystallization are sufficiently gradual to be treated as stationary (Figs 13 and 14). Figure 16 depicts the analysis results for the total, reversing, and nonreversing apparent heat capacity.

The reversing heat capacity was calculated as were the curves labeled I in Figs 13 and 14. The total heat-flow rate is approximated by the sliding average, described above and should be equal to the standard DSC result as long as the deconvolution from the reversing contribution is complete, i.e., the overall response is stationary. The curve labeled non-reversing is the difference between the total and the reversing heat-flow rate and is not based on additional measurement.

In Fig. 16, the small enthalpy relaxation in the glass transition region of PET shows better in the non-reversing heat-flow rate, and the increase of the heat capacity due to the glass transition in the reversing heat capacity, as expected from their difference in time scale. Additional information about this separation and the irrevers-

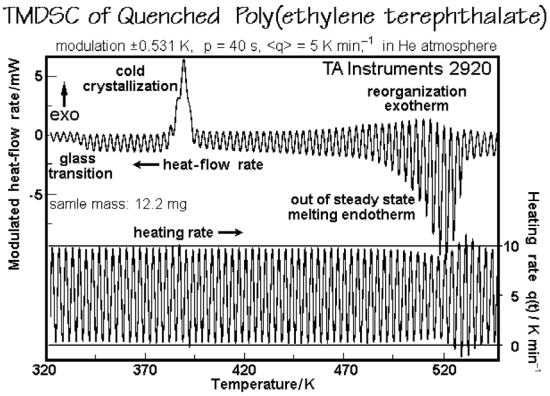

Fig. 15 Example TMDSC trace for poly(ethylene terephthalate), PET

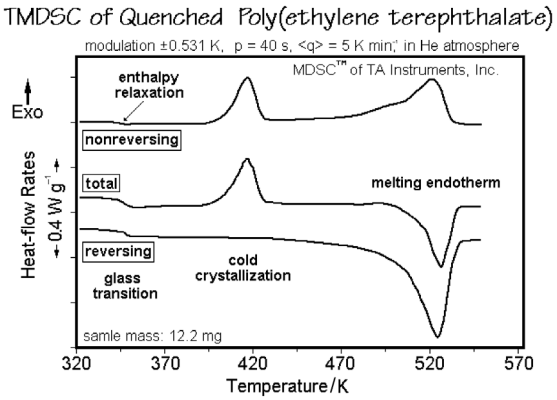

Fig. 16 Analysis of the data of Fig. 15

ibility of the glass transition itself will be mentioned in the discussion of Figs 22–24, below. Furthermore, the reversing and total heat capacities below 340 K and above 540 K are identical, i.e., they are fully reversible and expected to represent the thermodynamic heat capacity. The melting curve is, however, quite surprising. The polymer melting should be fully irreversible, but the reversing heat-flow rate is larger than the total. This makes the irreversible melting exothermic. Is this an indication of irreversible recrystallization and can it be quantitatively assessed? Before resolving this problem, it is of importance to remember that the heating rate did not quite follow the program because of instrument lags and that there is a good chance that both, the heating rate (a) and the heat-flow rate (b) are not stationary, causing errors on devonvolution into reversing and total rates.

A TMDSC analysis of indium is reproduced in Fig. 17. Indium is known to melt reversibly within at least ±0.05 K when in the presence of crystal nuclei. The heat-flow rate, $\Phi(t)$, reveals the first melting as a minor peak at position 1, followed by immediate recrystallization at 1'. In the subsequent cycle, the melting progresses to larger amounts before reversing the latent heat flow. The almost straight line between the melting and crystallization peaks is a measure of the instrument lag. Only after melting peak 7 are all crystals changed to liquid, and on cooling, no immediate crystallization occurs since there are no more nuclei are left. A supercooling of about 1.0 K is necessary before crystallization peak 7' appears. Of interest are also the deviations of the sample temperature shown at the bottom of Fig. 17. The sinusoidal modulation is interrupted in the melting range. During the melting and crystallization cycles, the sample temperature stays at T_m, and consequently, the measured temperature deviates strongly from the sinusoidal program, also shown in the figure.

The analysis of the first harmonic of the heat-flow rate is presented in Fig. 18. It cannot give quantitative information because of the loss of stationarity. The heat-flow rate is repeated as in Fig. 17 as the curve labeled $\Phi(t)$. The total heat-flow rate, $<\Phi(t)>$, is spread with small contributions at the time of each melting and crystallization peak. The major portion of the total latent heat between 103 and 104 min is

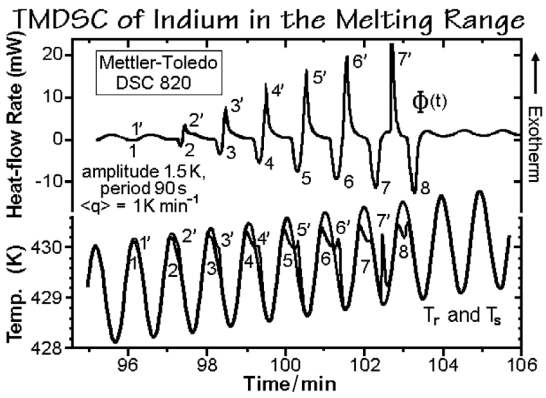

Fig. 17 Response of a TMDSC to the reversible melting of indium

broadened and not quantitative due to the averaging during the analysis. A better melting peak is seen in Figs 17 and 18 as peak 7 or 8, but must be separated from the sinusoidal baseline and then analyzed as shown in Fig. 9 or Fig. 10. The amplitude of the first harmonic of the heat-flow rate, $\langle A_\phi \rangle$, is influenced equally during melting and crystallization, i.e., due to each melting and crystallization cycles a latent heat is registered so that its area is many times that of $\langle \Phi(t) \rangle$, explaining qualitatively the larger reversing heat-flow rate for PET in Fig. 16. The conclusion that most of the reversing melting seen in Fig. 16 is actually irreversible, i.e., a given material melts and recrystallizes at different temperatures was drawn from quasi-isothermal experiments, similar to the ones shown for polyethylene in Figs 25 and 26, below [26]. They have shown that much, but not all, of the reversing melting is caused by errors in the data evaluation.

The question of handling of the empirical correction of frequency dependence of the heat capacity by TMDSC listed in Fig. 6 is illustrated with Figs 19 and 20 [27].

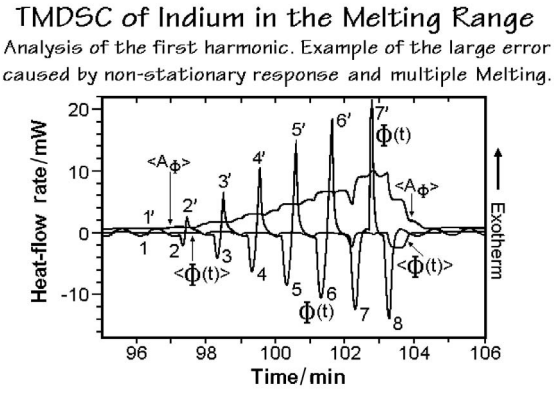

Fig. 18 Analysis of the data of Fig. 17

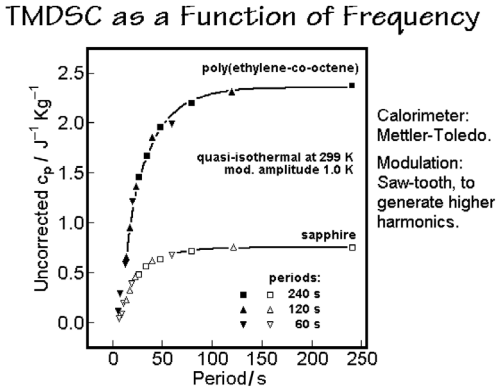

Fig. 19 Frequency dependence of a quasi-isothermal TMDSC analysis using three simple sawtooth modulations with the listed periods. The evaluation made use of the 1st, 3rd, 5th, 7th and 9th harmonics

Figure 19 shows the heat capacities of a poly(ethylene-co-octene), also known as linear, low-density polyethylene, and the calibrant sapphire (Al_2O_3) as a function of the period of modulation. The data are calculated using the equation of Fig. 6 without considering the square root, as is often suggested in the instrument manuals. Only with periods above about 200 s is the response independent of frequency. In Fig. 20 the data are plotted, so that their slopes give the value of τ. Up to a squared frequency of 0.2, which corresponds to a period, p, of about 15 s, τ is constant, as is expected if steady state, linearity, and stationarity are maintained [13], but even at higher frequencies corrections can be made if the function of τ is known. Since τ is different for sample and calibrant, a simple correction by measurement of sample and calibrant at the same frequency is not sufficient. Taking all precautions just discussed, heat capacities can be measured with TMDSC with higher precision than with DSC [15].

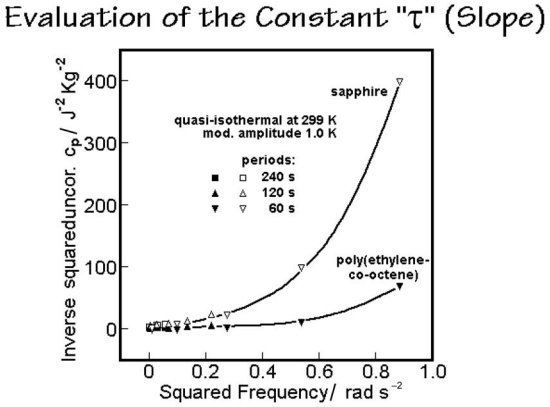

Fig. 20 Evaluation of the constant τ for the equation in Fig. 6 that is represented by the slope of the shown curves

Measurements and analyses in the glass transition region were made for amorphous polystyrene, PS, and semicrystalline PET [28–32]. Figure 21 shows the raw data and an enlarged plot of the analyzed results [32]. It looks as if the hysteresis and the glass transition response can be separated, as was already mentioned for PET in Fig. 16. Figures 22 and 23 illustrate the changes of the non-reversing and the reversing heat capacity in the glass transition region on samples with different thermal histories. From Fig. 23 it can be concluded that different thermal histories yield a different reversing glass transition kinetics at the same analysis frequency. Only if this (small) dependence of the kinetics on the thermal history is neglected, a separation of the two effects can be attempted. Naturally this separation will give results depending on the modulation frequency as well as on the thermal history. Furthermore, by using simple models of the glass transition, it became clear that the first harmonic used for the analysis is not a quantitative representation of the overall response of the sample. By not considering higher harmonics, the non-reversing heat capacity contains some of these reversing effects. A simple hole model for the glass transition, as suggested by Hirai and Eyring for example [33], using first-order kinetics, was developed a number of years ago [34]. It is too simple to represent the glass transition quantitatively, mainly because of the missing cooperativity [35]. It, however, has been used to use the experimental first harmonic to calculate the actual kinetics, including all terms of the Fourier series for the model. This calculation yields the number of high-energy conformations in a TMDSC cooling experiment, as shown in Fig. 24 [31]. At sufficiently high temperature for the considered modulation frequency, the response is that of a liquid. A fully reversible response to the modulation is calculated. On cooling, the fast modulation effect is seen to freeze at some temperature, but a slower effect, due to the underlying cooling rate, freezes more gradually at lower temperature and gives rise to the enthalpy relaxation on heating at faster heating rates, as also shown in [31]. Furthermore, within this model, one can make a quantitative evaluation of the enthalpy relaxation, pointing to the improvement in the

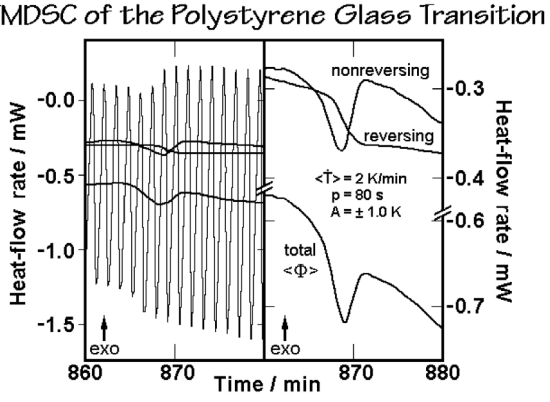

Fig. 21 Analysis of the glass transition of polystyrene by TMDSC [31]

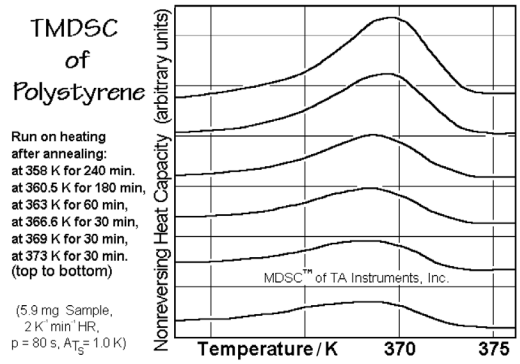

Fig. 22 Separation of the enthalpy relaxation, data as in Fig. 21

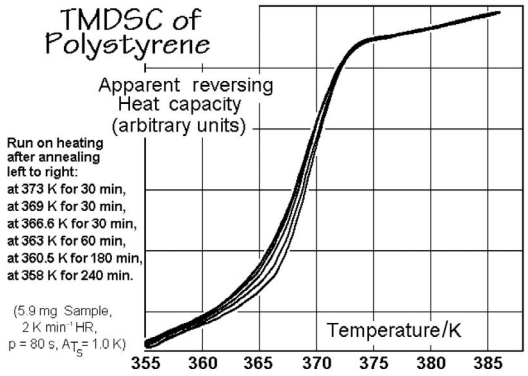

Fig. 23 Separation of the apparent reversing heat capacity, data as in Fig. 21

theory of the glass transition needed before a quantitative analysis of the kinetics of the glass transition becomes possible.

Analyzing the glass transition of semicrystalline PET, one can see, in addition, a reduction in the activation energy of the transition and a separation of the glass transition of the rigid amorphous fraction, RAF [28]. The rigid amorphous fraction was shown to develop on crystallization, and either has a glass transition below the melting temperature, or it softens parallel with the melting of the crystals [26].

The most interesting observation is by quantitative TMDSC of semicrystalline, flexible polymers. They show not only the reversing heat capacity which originates from incomplete deconvolution, irreversible recrystallization, and instrument lag, but after accounting for all of these non-reversible effects, there remains an apparent excess heat capacity due to the latent heat of reversible melting [26, 36]. Figure 25 illustrates this point with a comparison of a standard DSC trace of melt-crystallized polyethylene with a series of quasi-isothermal TMDSC results. In the latter measurements modulations were

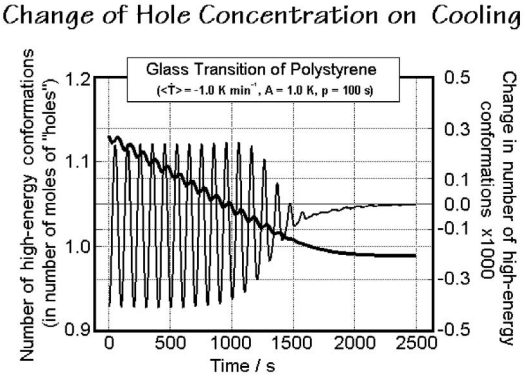

Fig. 24 Data analysis in terms of 'hole' concentrations (data of Fig. 21)

carried out about a constant base temperature for 20 min or more. After a constant apparent reversing heat capacity was approached, the measurement was begun. In the center of the melting peak the waiting time had sometimes to be extended, and ultimately extrapolated to infinite time. When all slow irreversible processes had decayed, results as shown in Fig. 25, and expanded in Fig. 26, were seen. The open symbols in Fig. 26 show a dependence of this reversible melting on the thermal history imparted before the series of quasi-isothermal runs on heating was undertaken, and the filled circles show that on cooling from the melt, immediately after crystallization, the reversible melting is less. Much of the reversible melting material forms only at lower temperature through annealing. The comparison to the thermodynamic heat capacity derived outside the transition region shows that the range of this melting is more than 100 K and stretches well into the range of practical applications of polyethylene. Figure 26 documents also that the fraction of reversible melting at low temperature approaches that of the total melting. Two explanations have been derived for this reversible melting. One was that this reversible melting is connected with the earlier observed reversible change in lamellar thickness [37], which was later connected to the gauche-defect equilibrium, discussed above [22, 26]. The other involves the melting on the crystal growth faces, the reverse of crystallization [36]. Both explanations were documented not only with DSC and TMDSC, but also by time-resolved X-ray scattering [38, 39]. Polymers without mobile defects do not anneal to larger fold length below the melting temperature and seem to show mainly growth-face reversible melting. Furthermore, rather rigid polymers, like polycarbonates and poly(oxyphenylene)s show little or no reversible melting [26, 40].

Figure 27 shows results of melting experiments on extended-chain paraffins and chain-folded crystals of large molar mass, crystallized to rather thin lamellar crystals [5]. These two curves, expressed by the empirical equations in the figure, set the limits of a whole series of melting points of crystals with one or more folds and their corresponding molecular length [41]. Knowing that sufficiently long sequences of crystallizable units can crystallize and melt at temperatures that are close to isolated molecules of the same length [5], one needs only the concept of decoupling of chain

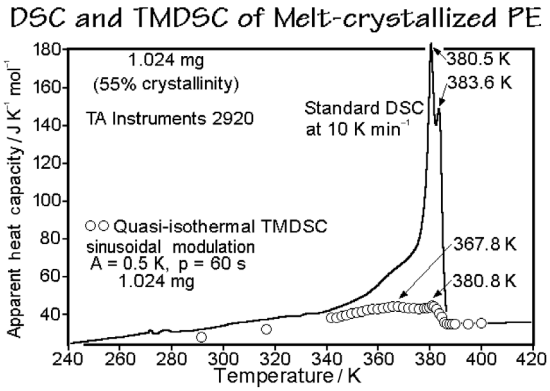

Fig. 25 Melting of polyethylene by DSC and TMDSC

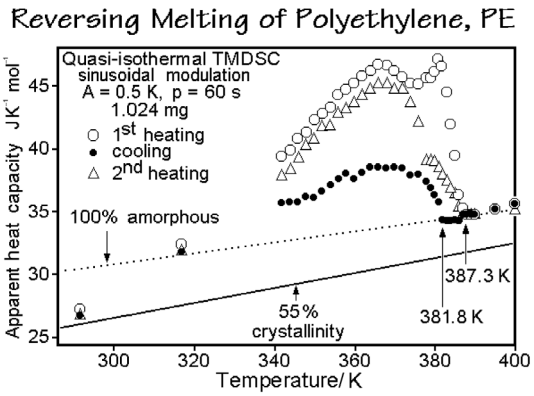

Fig. 26 Enlargement of the reversing melting by TMDSC shown in Fig. 25

segments in semicrystalline polymers at the phase-boundaries to explain a broad range of reversible or nearly reversible melting temperatures [42]. This concept of decoupling of chain segments is shown schematically in Fig. 28. Reversibility can in this case be maintained as long as a molecular nucleus remains on the growth face [43].

The application of TMDSC, thus, yields a new picture for semicrystalline polymers. The overall structure is that of a globally metastable aggregate of micro- and nanophases with most molecules extending across the phase boundaries. The micro- and nanophases can be crystalline, liquid, or glassy. Mesophases are also possible as part of the semicrystalline polymer structure, as indicated in Fig. 1. A rigid amorphous phase may be separated from the mobile amorphous phase [7]. Within this non-equilibrium phase structure, reversible processes can occur on the crystal growth faces or on their fold surfaces. Heating and cooling of such structure is accompanied by a large variety of processes, extending over wide temperature ranges and encom-

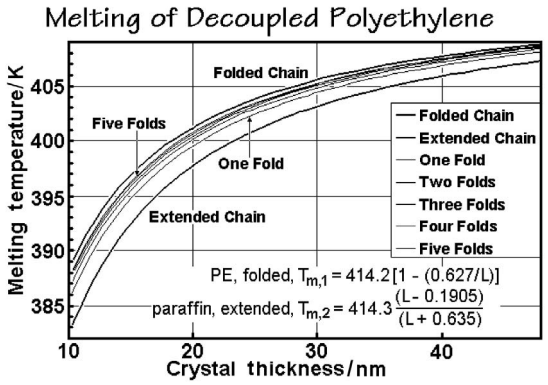

Fig. 27 Melting temperatures of polyethylene [5]

passing irreversible and reversible melting/crystallization, disordering/perfection, and glass transitions.

The question that remains to be discussed is the possibility of attaining a global equilibrium of melting and crystallization. Figure 29 shows the DSC and quasi-isothermal TMDSC of extended-chain crystals of polyethylene with a crystallinity close to one [44]. Such materials can be made by crystallization at elevated pressure into the hexagonal crystal mesophase [2]. In this phase the initially grown folded-chain morphology anneals quickly to a close-to-equilibrium structure. Although the crystallization is not an equilibrium path, the final product is in equilibrium. Melting of these equilibrium crystals occurs at the equilibrium melting temperature if enough time is allowed to avoid superheating. The reverse of this melting process, however, is not possible because of the supercooling needed to overcome crystal and molecular nucleation barriers [43]. In agreement with this long-known behavior [5], Fig. 29

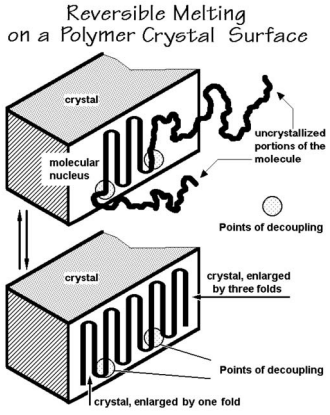

Fig. 28 Reversible melting of decoupled parts of a flexible macromolecule

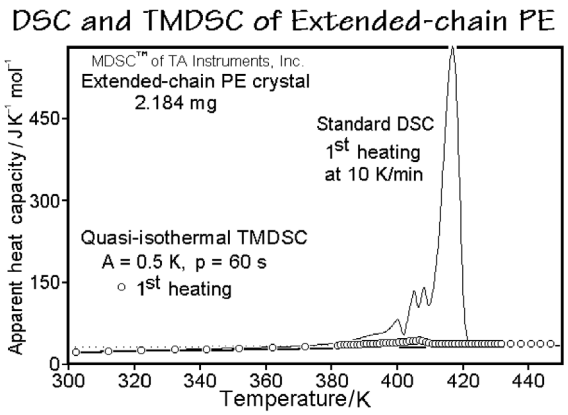

Fig. 29 Melting of extended chain, equilibrium crystals of polyethylene by DSC and TMDSC

shows practically no reversible melting. The minor amount of excess reversible apparent heat capacity has been quantitatively accounted for by the presence of a small amount of low molar mass polyethylene [44]. The breadth of the melting and premelting peaks have also been linked to superheating and separation of low molar mass fractions, respectively. One can conclude that equilibrium crystals of polyethylene melt irreversibly.

Starting from the well-established equilibrium crystal of short chain paraffins, TMDSC proves in Fig. 30 that their melting is fully reversible only up to a molar mass of about 1 000 Da [45]. This mass corresponds to a lamellar thickness of 9.0 nm, or $x \approx 70$ in Fig. 30, much less than is needed for the beginning of chain folding.

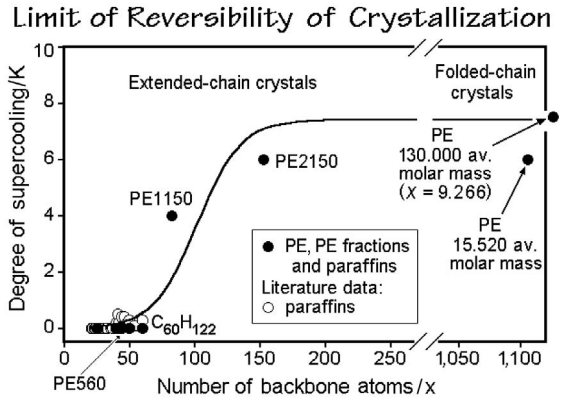

Fig. 30 Change of melting of paraffins and polyethylene from reversible to irreversible melting

Conclusions and the Future of Thermal Analysis

The tribulations of thermal analysis in the 20th century are most salient in the stages of development of quantitative measurement of heat. The DTA was established 100 years ago and showed that it may be possible to measure heat quantitatively. The biggest application was unfortunately the analysis of phase transitions via quantitative determination of the transition temperatures only. Little use was made of quantitative measurements of heat. With the development of the DSC and the interpretation of heat capacity in terms of molecular motion, thermal analysis had reached maturity. Calorimetry could now be done by DSC and, in time, the precision at temperatures above 200 K approached or exceeded that of the classical adiabatic calorimetry. Again, despite the great importance of the information that could be generated from quantitative measurements of heat and its link to molecular motion, the largest volume of DSC data published followed DTA tradition and remained qualitative.

The biggest application of the DSC was in the field of polymer science (>50%), and there, it was found that many of the thermal analyses dealt with irreversible processes. The invention of a commercial TMDSC provided the ideal tool to distinguish reversible and irreversible changes. The step from DSC to TMDSC required not only to keep up calibration and handling of the lag-caused effects to a higher standard, but now it became also necessary to develop proper analysis methods in form of Fourier analyses and proper deconvolution of the reversing and total effects. Not only must questions about instrument lag, steady state, linearity, and calibration be answered, as understood for DSC, TMDSC needs also to find answers for the effects of frequency and amplitude, stationarity, and multiple harmonics. The thermal analyst must keep up with all these points, but the successes briefly outlined in the previous section make this added effort well worth-while.

Perhaps one should look into the future of thermal analysis [46]. Where should the development of thermal analysis go? There is no question that the largest progress could be obtained by changing the excessive volume of qualitative data to true calorimetry, followed by an interpretation in terms of molecular motion and phase structure. Advances in other areas is most certainly going to the direct thermal analysis of nanophases and surfaces that make up much of present-day cutting edge research [47, 48]. In many applications the actual thermal processes are much faster than is possible to follow with most DSC and TMDSC. Rates as high as 1 000 K s^{-1} may be needed for many applications. Initial efforts are available in this exciting area which also needs further development to become a quantitative calorimetric technique [49–52].

* * *

This work was supported by the Division of Materials Research, National Science Foundation, Polymers Program, Grant # DMR-0312233. Use of some of equipment and laboratory space was provided by the Division of Materials Sciences and Engineering, Office of Basic Energy Sciences, U.S. Department of Energy at Oak Ridge National Laboratory, managed and operated by UT-Battelle, LLC, for the U.S. Department of Energy, under contract number DOE-AC05-00OR22725.

'The submitted manuscript has been authored by a contractor of the U.S. Government under the contract No. DOE-AC05-00OR22725. Accordingly, the U.S. Government retains a non-exclusive, royalty-free license to publish or reproduce the published form of this contribution, or allow others to do so, for U.S. Government purposes.'

References

1 Most of the topics of this paper are based on the computer course: Thermal Analysis of Materials, downloadable from the internet: *web.utk.edu/~athas/courses/tham99.html*, on the earlier book B. Wunderlich, Thermal Analysis, Academic Press, Boston 1990, on Chapter 2 of E. Turi, Ed., Thermal Characterization of Polymeric Materials. Academic Press, New York, revised 2nd ed., 1997, and the book in preparation: Thermal Analysis of Polymeric Materials. Springer, Berlin scheduled for 2005.
2 B. Wunderlich and J. Grebowicz, Adv. Polymer Sci., 60/61 (1984) 1.
3 B. Wunderlich, Thermochim. Acta, 340/41 (1999) 37.
4 W. Chen and B. Wunderlich, Macromol. Chem. Phys., 200 (1999) 283.
5 B. Wunderlich, Macromolecular Physics, Volume 3, Crystal Melting, Academic Press, NewYork, 1980.
6 B. Wunderlich, Thermochim. Acta, 403 (2003) 1; J. Thermal Anal., 49 (1997) 513.
7 H. Suzuki, J. Grebowicz and B. Wunderlich, British Polymer Journal, 17 (1985) 1.
8 See W. J. Smothers and Y. Chiang, Handbook of Differential Thermal Analysis, Chem. Publ. Co., New York 1966.
9 B. Wunderlich, Thermal Analysis, Academic Press, New York, 1990.
10 E. S. Watson, M. J. O'Neill, J. Justin and N. Brenner, Anal. Chem., 36 (1964) 1233.
11 P. S. Gill, S. R. Sauerbrunn and M. Reading, J. Thermal Anal., 38 (1992) 931.
12 B. Wunderlich, A. Boller, I. Okazaki, K. Ishikiriyama, W. Chen, M. Pyda, J. Pak, I. Moon and R. Androsch, Thermochim. Acta, 330 (1999) 21.
13 B. Wunderlich, Y. Jin and A. Boller, Thermochim. Acta, 238 (1994) 277.
14 R. Androsch, I. Moon, S. Kreitmeier and B. Wunderlich, Thermochim. Acta, 357/358 (2000) 267.
15 J. Pak and B. Wunderlich, Thermochim. Acta, 367/368 (2001) 229.
16 E. Turi, Ed., 'Thermal Characterization of Polymeric Materials.' Academic Press, New York, revised 2nd Ed., 1997.
17 V. B. F. Mathot, Ed., Calorimetry and Thermal Analysis of Polymers, Hanser Publishers, Munich 1993.
18 S. Z. D. Cheng, Ed., Handbook of Thermal Analysis and Calorimetry, Vol. 3, Applications to Polymers and Plastics, Elsevier Science, Amsterdam 2002.
19 B. Wunderlich, Thermochim. Acta, 300 (1997) 43.
20 B. Wunderlich, The ATHAS Data Base on Heat Capacities of Polymers, Pure Applied Chem., 67 (1995), 1019. For data, see our website: *http://web.utk.edu/ ~athas*.
21 G. L. Liang, D. W. Noid, B. G. Sumpter and B. Wunderlich, J. Phys. Chem., 98 (1994) 11739.
22 B. G. Sumpter, D. W. Noid, G. L. Liang and B. Wunderlich, Adv. Polymer Sci., 116 (1994) 27.
23 M. Reading, Ed., Basic Theory and Practice for Modulated Temperature Differential Scanning Calorimetry (MTDSC), Kluwer Academic Publishers, Dordrecht, The Netherlands, 2004.

24 A. T. Riga and L. H. Judovits, Eds, Material Characterization by Dynamic and Modulated Thermal Analytical Techniques, *ASTM STP 1402*, American Society for Testing and Materials, West Conshohocken, PA 2001.
25 B. Wunderlich, J. Thermal Anal., 48 (1997) 207.
26 B. Wunderlich, Progress in Polymer Science, 28 (2003) 383.
27 R. Androsch and B. Wunderlich, Thermochim. Acta, 333 (1999) 27.
28 B. Wunderlich and I. Okazaki, J. Thermal Anal., 49 (1997) 57; J. Polym. Sci., Part B: Polymer Phys., 34 (1996) 2941.
29 L. C. Thomas, A. Boller, I. Okazaki and B. Wunderlich, Thermochim. Acta, 291 (1997) 85.
30 A. Boller, I. Okazaki and B. Wunderlich, Thermochim. Acta, 284 (1996) 1.
31 B. Wunderlich, A. Boller, I. Okazaki and S. Kreitmeier, J. Thermal Anal., 47 (1996) 1013.
32. A. Boller, C. Schick and B. Wunderlich, Thermochim. Acta, 266 (1995) 97.
33 H. Hirai and H. Eyring, J. Polymer Sci., 27 (1959) 51.
34 B. Wunderlich, D. M. Bodily and M. H. Kaplan, J. Appl. Phys., 35 (1964) 95.
35 J. M. Hutchinson, J. Therm. Anal, Cal., 72 (2003) 619.
36 I. Okazaki and B. Wunderlich, Macromolecules, 30 (1997) 1758.
37 E. W. Fischer, Pure Appl. Chem., 31 (1972) 113.
38 B. Goderis, H. Reynaers, R. Scherrenberg, V. B. F. Mathot and M. H. J. Koch, Macromolecules, 34 (2001) 1779.
39 R. Androsch, J. Blackwell, S. N. Chvalun and B. Wunderlich, Macromolecules, 32 (1999) 3735.
40 S. Montserrat, F. Roman and P. Colomer, J. Therm. Anal. Cal., 72 (2003) 657.
41 R. Androsch and B. Wunderlich, J. Polym. Sci., Part B: Polym. Phys., 41 (2003) 2157, 2039.
42 B. Wunderlich, J. Polym. Sci., Part B: Polym. Phys., 42 (2004) 1275.
43 B. Wunderlich and A. Mehta, J. Polym. Sci., Polym. Phys. Ed., 12 (1974) 255.
44 J. Pak and B. Wunderlich, J. Polym. Sci., Part B: Polym. Phys., 40 (2002) 2219.
45 J. Pak and B. Wunderlich, Macromolecules, 34 (2001) 4492.
46 B. Wunderlich, Thermochim. Acta, 355 (2000) 43.
47 I. Moon, R. Androsch, W. Chen and B. Wunderlich, J. Therm. Anal. Cal., 59 (2000) 187.
48 M. Y. Efremov, E. A. Olson, M. Zhang and L. H. Allen, Thermochim. Acta, 403 (2003) 37.
49 E. Hellmuth and B. Wunderlich, J. Appl. Phys., 36 (1965) 3039.
50 N. E. Hager, Rev. Sci. Instrum., 43 (1972) 1116.
51 Z. Q. Wu, V. L. Dann, S. Z. D. Cheng and B. Wunderlich, J. Thermal Anal., 34 (1988) 105.
52 S. A. Adamovsky, A. A. Minakov and C. Schick, Thermochim. Acta, 403 (2003) 55.